ACS APPLIED MATERIALS & INTERFACES

Research Article

www.acsami.org

Different Interaction Modes of Biomolecules with Citrate-Capped Gold Nanoparticles

Shiyun Zhang, Yasmine Moustafa, and Qun Huo*

NanoScience Technology Center, Department of Chemistry, College of Science, and Burnett School of Biomedical Science, College of Medicine, University of Central Florida, 12424 Research Parkway, Suite 400, Orlando, Florida 32826, United States

Supporting Information

ABSTRACT: In this study, we investigated the interaction between five biorelevant molecules and citrate-capped gold nanoparticles using dynamic light scattering, ζ-potential analysis, UV−vis absorption spectroscopy, and transmission electron microscopy. The five biomolecules are bovine serum albumin (BSA), two immunoglobulin G (IgG) proteins, immunoglobulin M (IgM), and a polysaccharide molecule, hyaluronan. BSA, IgG, and IgM are high abundance proteins in blood. Hyaluronan is a major component of the extracellular matrix. An abnormal level of hyaluronan in blood is associated with a number of medical conditions including rheumatoid arthritis and malignancy. Five different interaction modes were observed from these molecules. While BSA and IgM interact with the gold nanoparticles by forming electrostatic interactions with the citrate ligands, IgG and hyaluronan adsorb to the nanoparticle metal core by displacing the citrate ligands. BSA, rabbit IgG, and hyaluronan formed a stable monolayer on the nanoparticle surface. Human IgG and IgM caused nanoparticle cluster formation upon interacting with the gold nanoparticles. For the first time, we discovered that hyaluronan, a highly negatively charged polyglycosaminoglycan, exhibits an exceptionally strong affinity toward the citrate−gold nanoparticles. It can effectively compete with IgG to adsorb to the gold nanoparticles. This finding has exciting implications for future research: the molecular composition of a protein corona formed on a nanoparticle surface upon mixing the nanoparticle with blood or other biological fluids may vary according to the pathological conditions of individuals, and the analysis of these compositions could potentially lead to new biomarker discovery with diagnostic applications.

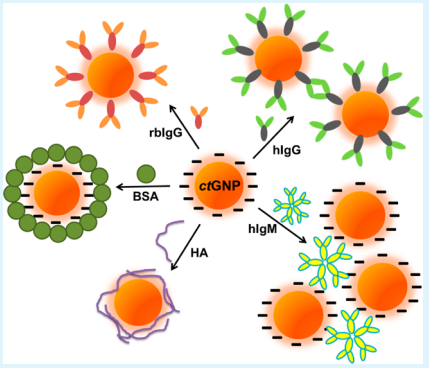

KEYWORDS: *gold nanoparticle, protein corona, protein−nanoparticle interaction, dynamic light scattering, polysaccharides, hyaluronan*

INTRODUCTION

Citrate-capped gold nanoparticles (*ct*GNPs), also known as gold colloids, can be prepared conveniently using Turkevich or modified Turkevich method in large quantity and high quality.[1−4] Because such particles are made in aqueous solution, they can be readily applied for biological studies and applications following conjugation with various biomolecules.[5,6] Like other nanoparticle materials, many proteins readily adsorb to *ct*GNPs through noncovalent interactions to form a so-called "protein corona".[7−13] This simple physical adsorption process has been widely used to prepare gold nanoparticle bioconjugates, especially gold immunoprobes for immunohistology analysis and in vitro diagnostics.[14−16]

To further extend the application of gold nanoparticles in both in vitro and in vivo systems, the study of interactions between different biomolecules, especially biomolecules existing in the blood and gold nanoparticles becomes more important. Such studies are not only necessary to help better understand the activity and potential toxicity of gold nanoparticles in the biological systems but also may lead to new diagnostics and personalized medicine. Our blood system contains thousands to tens of thousands of different proteins and other types of biomolecules including polysaccharides, DNAs, RNAs, lipids, and small molecular metabolites.[17,18] Studies reported so far by a number of research groups have identified more than 50 blood proteins adsorbed to the *ct*GNPs.[10,11] In addition to proteins, lipids molecules were also found in the protein corona.[7] The composition and relative quantity of biomolecules existing in the blood are affected by the physiological and medical conditions of each individual.[19−21] Therefore, it is possible that the types and amounts of biomolecules adsorbed to the *ct*GNPs could also vary from person to person, reflecting the medical conditions and status of individuals. We recently discovered from the study of animal models and prostate cancer patients that the presence of a prostate tumor can change how serum proteins interact with *ct*GNPs.[22,23] By studying and analyzing the specific biomolecules adsorbed to the *ct*GNPs, new molecular biomarkers may be identified for diagnostic applications.

Received: September 8, 2014
Accepted: October 27, 2014
Published: October 27, 2014

 © 2014 American Chemical Society

Despite extensive research and studies conducted on *ct*GNPs, our understanding on how various biomolecules interact with *ct*GNPs remains rather limited. The *ct*GNP has two structural components that can contribute to the chemical interactions with biomolecules: the metal core surface and the citrate ligands. One fundamental question yet to be clarified is during the interaction, does the biomolecule bind with the metal core or with the citrate ligands, or through both? Another more practical question is how to evaluate the relative binding of various biomolecules with the *ct*GNPs, especially in a mixture of biomolecules. Such analysis may help predict and determine the composition of the "biomolecular corona" formed on the nanoparticle surface in complex biological fluids such as blood serum. Also, while most studies conducted so far were focused on proteins, much less attention has been paid on the interaction of other types of biomolecules, such as polysaccharides with the *ct*GNPs. Similar to proteins, polysaccharides represent a major structural and functional component of the biological system, especially in the extracellular matrix. It is important to consider polysaccharides in the overall context of biomolecule−*ct*GNP interactions.

In this study, we investigated the interactions between five different biomolecules and *ct*GNPs: bovine serum albumin (BSA), two immunoglobulin G (IgG) proteins, human immunoglobulin M (hIgM), and a negatively charged polysaccharide, hyaluronan (HA). Serum albumin is one of the most abundant blood proteins. BSA has been used as a model protein in several studies to examine the protein-*ct*GNP interactions.[24−29] We include BSA in the study for comparison purpose. IgG and IgM are also abundant blood proteins. Although a typical IgG is an immunoglobulin monomer, IgM is a pentamer of immunoglobulin protein. Among the two IgG proteins included in this study, one is a rabbit IgG (rbIgG) and one is human IgG (hIgG). Although rbIgG is a monomer, human IgG purified from pooled human blood donors is known to contain a certain percentage (up to ∼40%) of dimers and oligomers.[30−32] We shall demonstrate in our study that even the same type of protein could interact with nanoparticles quite differently. Hyaluronan (HA) is a major component of the extracellular matrix (ECM). Extensive research and evidence have shown that HA is associated with various cancer development including prostate and bladder cancer.[33−37] In reference to our recent finding of prostate tumor-induced changes in the blood serum−*ct*GNP interaction products,[22,23] we asked a question if HA is a tumor-associated molecule that could have caused these changes. Studies have been reported on covalently conjugating HA to *ct*GNP as a drug delivery system or for in vivo diagnosis and imaging purposes.[38−40] However, to our best knowledge, no study has been reported on the noncovalent interaction between HA and *ct*GNP, and more importantly, if and how the presence of HA may affect the adsorption of other serum proteins with the *ct*GNP.

From this study, we discovered that different biomolecules can have different interaction modes with the *ct*GNP. In particular, with regard to BSA, rbIgG, hIgG, hIgM, and HA, we found the following interaction modes, as illustrated in Figure 1: (1) BSA forms a highly stable, monolayer-like protein corona on the GNP surface through electrostatic interaction with the negatively charged ligands on the nanoparticle surface, (2) IgG (both rbIgG and hIgG) interacts with *ct*GNPs by displacing the citrate ligands and binding with the nanoparticle metal core, (3) while monomeric rbIgG forms a monolayer-like protein corona on the GNP surface, hIgG causes an irreversible coalescence of the GNPs into large aggregates, (4) hIgM interacts with the *ct*GNPs through the citrate ligands and cross-links *ct*GNPs into nanoparticle clusters but not aggregates, and finally (5) HA binds directly to the GNP metal core by displacing the citrate ligands, forming a polysaccharide coating on the GNP surface. The interaction of HA with *ct*GNP was found to be dependent on the molecular weight of HA. Furthermore, from the competitive adsorption studies, we discovered that HA has a high affinity with the *ct*GNPs. HA, especially the high molecular weight HA, can compete with IgG to bind with the *ct*GNPs at a significantly lower concentration than IgG.

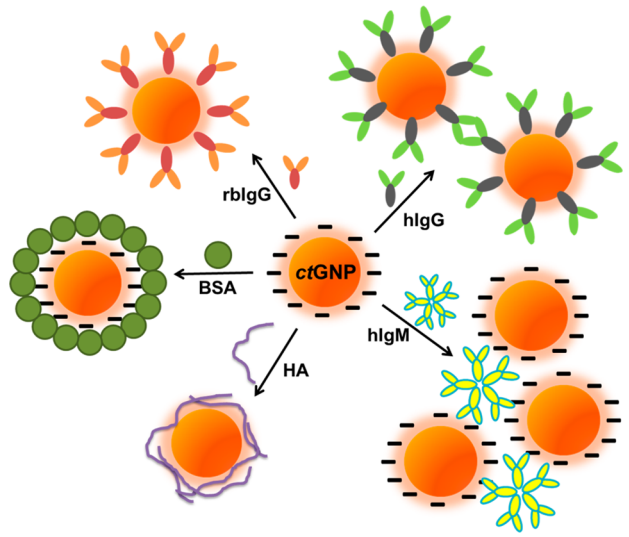

Figure 1. Illustration of five different interaction models between BSA, rabbit IgG (rbIgG), human IgG (hIgG), human IgM (hIgM), and hyaluronan (HA) with *ct*GNP.

Our study reveals that biomolecular interaction with *ct*GNPs is a rather complicated process controlled by many factors. Multiple experimental approaches need to be used to understand the different interaction modes. For the first time, we demonstrate that tumor-associated molecules could compete with blood proteins and biomolecules to bind with *ct*GNPs, therefore, changing the composition profile of the protein corona formed on the nanoparticle surface. This finding pointed out an interesting new opportunity in nanoparticle research: by analyzing the molecular composition of protein coronas formed on the nanoparticle surface, new molecular biomarkers specific to certain diseases and medical conditions may be discovered.

RESULTS AND DISCUSSION

Particle Size and ζ-Potential Analysis. Dynamic light scattering (DLS) was used here as the primary tool to study the biomolecule−GNP interaction. Most biomolecules are large molecules with a hydrodynamic diameter varying from a few nanometers to 100s of nanometers. As many studies have shown previously, when a layer of biomolecules is adsorbed to the nanoparticles, the average particle size is expected to increase and this size increase is readily measurable by DLS.[10,24,41−43] The typical molecular weight of BSA, IgG, and IgM is around 60, 150, and ∼750 kDa. HA as a polysaccharide and can have different molecular weights. Four molecular weights of HA were chosen for this study: a high molecular weight of 1.5 million Da (HAH), a medium size of 289 kDa (HAM), a low molecular weight of 29 kDa (HAL),

and an ultralow molecular weight of 7 kDa (HAU). A *ct*GNP product from Ted Pella with an average hydrodynamic diameter of 92−95 nm at a concentration of 10 pM was used throughout the whole study.

Figure 2A is the average particle size of the nanoparticle solution upon mixing with the five different biomolecules, respectively. HA used in this study is the medium molecular weight HAM. In general procedure, 2 μL of biomolecule solution at a concentration of 1 mg/mL was mixed with 40 μL *ct*GNP solution. The final molar concentration of BSA, rbIgG, hIgG, hIgM, and HA in the nanoparticle mixture solution is approximately 18.0, 6.0, 6.0, 1.2, and 3.0 μM, respectively. The lowest protein concentration, which is hIgM solution, is 120 000 times in excess over the gold nanoparticle concentration (10 pM). Therefore, it can be considered that all the nanoparticle adsorption studies were performed under saturated biomolecular concentration. Following a 6 min of incubation time at room temperature, the particle size was measured. For BSA and rbIgG, the average particle size increased by about 10 and 20 nm, respectively. These numbers are in line with previous reports by us and other groups,[24,41−43] and also agree with the hydrodynamic diameter of BSA and IgG monomer of 5 and 10 nm as determined by other methods.[44,45] The determined "protein corona" thickness corresponds to the size of BSA and monomer IgG adsorbed to the GNPs. This also suggests that BSA and rbIgG formed a monomolecular layer on the GNP surface.

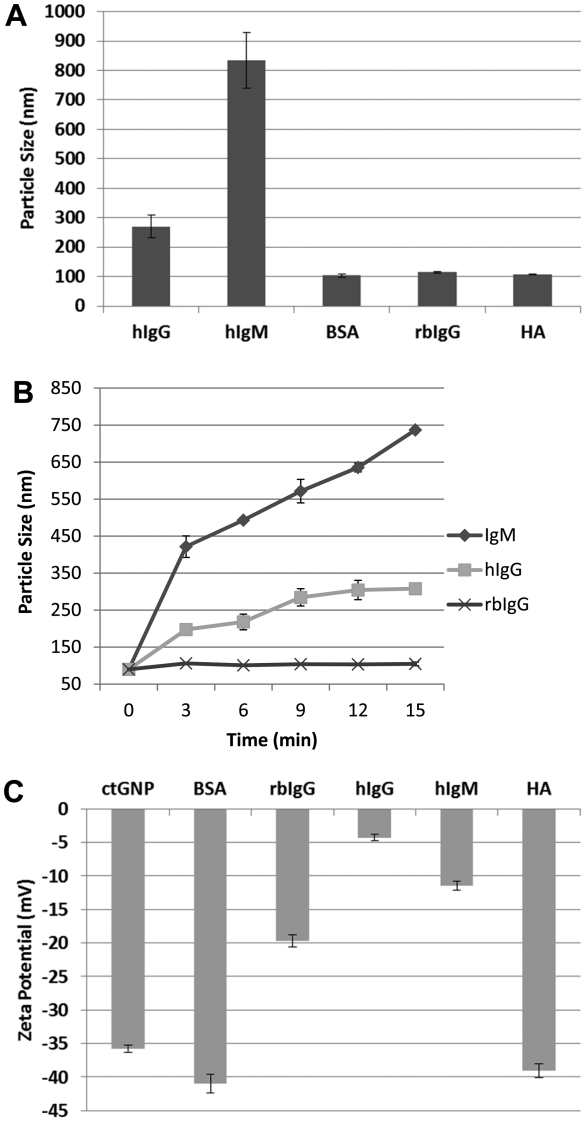

Figure 2. Size and ζ-potential of biomolecule−*ct*GNP interaction products. (A) Dynamic light scattering analysis. Mixed biomolecule−*ct*GNP solution was prepared by adding 2 μL of biomolecule solution at a weight concentration of 1 mg/mL with 40 μL of *ct*GNP solution (95 nm, 10 pM). The average particle size of the mixed solution was measured following a 6 min of incubation. (B) Time-dependent adsorption study of rbIgG, hIgG, and hIgM with *ct*GNP. The relative amount of protein and *ct*GNP in the study is the same as used in panel A). (C) ζ-Potential analysis. Mixed biomolecule−*ct*GNP solution was prepared by adding 2 μL of biomolecule solution at a weight concentration of 1 mg/mL with 600 μL of *ct*GNP solution. ζ-Potential was measured following a 6 min of incubation time. HA used in this study is a medium molecular weight HAM.

The interaction of HA with GNP is rather unique. Despite the relatively large molecular weight of HA used in this study, 289 kDa, which is almost 2 times the molecular weight of an IgG monomer (150 kDa), the adsorption of HA to *ct*GNP only led to a particle size increase of ∼10 nm (Figure 2A). HA is a linear polyglycosaminoglycan (GAG) with one carboxylate group per monomer unit.[33] Therefore, HA is highly negatively charged under physiological pH conditions. Literature reports suggest that HA adopts a linear, semiflexible conformation.[47] Because HA is also highly negatively charged, it can be assumed that HA does not adsorb to the *ct*GNPs by interacting with the citrate ligands. The only possible mode for HA to interact with *ct*GNP is to displace the citrate ligands and "wrap around" the gold nanoparticles with an extended chain conformation as illustrated in Figure 1. In other words, HA must interact with the *ct*GNP through the metal core.

The ζ-potential analysis revealed different surface charges of the GNPs treated with the five biomolecules (Figure 2C). To perform the study, 2 μL of biomolecule solution was mixed with 600 μL of *ct*GNP. After a few minutes of incubation time, the ζ-potential was measured. The ζ-potential of *ct*GNP is about −36 mV. Following the adsorption of BSA, rbIgG, hIgG, hIgM, and HA, the ζ-potential of the nanoparticle became −40,

−20, −4, −11, and −40 mV, respectively. The *ct*GNP is suspended in pure water with a pH of 5−6. In a control experiment, a same amount of biomolecule solution was added to 600 μL pure water. ζ-Potential measurement on these control solutions cannot be performed because the scattering intensity of the solution is too weak. The photon count rate of pure biomolecule solutions is less than 1−2 kcps and the count rate of *ct*GNP and mixed biomolecule−*ct*GNP solutions is a few hundreds kcps (kilo-counts per second). This control experiment confirmed that the ζ-potential measured from the biomolecule−*ct*GNP mixed solution is from the biomolecule-modified *ct*GNP, not a sum effect of *ct*GNP plus the biomolecule. The ζ-potential data alone does not provide direct information on the interaction modes between the five biomolecules and the *ct*GNP. However, in combination with the results as discussed in the following sections, ζ-potential measurement provides additional supporting evidence on certain interaction modes and mechanisms.

UV−Vis Absorption Spectroscopy and Transmission Electron Microscopy (TEM) Analysis. The UV−vis absorption spectra revealed several differences between the five biomolecule-treated *ct*GNPs (Figure 3A). The interaction of *ct*GNP with BSA, HA, and rbIgG led to only a few nanometers of red shift in the surface plasmon resonance (SPR) wavelength. The interaction with hIgM caused an approximately 15 nm red shift and slight broadening of the SPR band. In contrast, the interaction of hIgG led to significant broadening of the SPR band and a red shift of λmax by more than 40 nm. It is interesting to note that despite the larger particle size of the hIgM−*ct*GNP mixture as detected by DLS, hIgG−*ct*GNP exhibits a more significant level of nanoparticle cluster or aggregate formation according to the SPR band shift. This is further confirmed by TEM analysis. Representative TEM images show that the nanoparticles following hIgG treatment are severely coalesced together into large aggregates (Figure 3B,C), while the nanoparticles in the hIgM−*ct*GNP mixture are clustered together, but with a well-defined gap between the nanoparticles (Figure 3D,E). The average particle−particle distance of the nanoparticle clusters found in the hIgM−*ct*GNP mixture is about 20 nm, close to the estimated diameter of hIgM. Additional low magnification TEM images of *ct*GNP, hIgG−*ct*GNP, and hIgM−*ct*GNP interaction products are included in the Supporting Information (Figure S2).

To explain the difference between hIgG and hIgM, we propose the following reasoning. During the interaction between hIgG and *ct*GNP, the citrate ligand layer is destroyed or partially destroyed, leading to the exposure of the gold nanoparticle metal core. Before a complete hIgG monolayer is formed on the nanoparticle surface, the hIgG dimer/oligomer brings the "naked" gold nanoparticles together and strong van der Waals interactions between such nanoparticles cause an irreversible coalescence of the nanoparticles into large aggregates. In contrast, hIgM cross-links *ct*GNPs through electrostatic interactions with the citrate ligands. The gold nanoparticles remain covered by the citrate ligand layer during the interaction; therefore, no coalescence would occur.

Competitive Binding of Hyaluronan (HA) over hIgG with *ct*GNP. Through competitive adsorption study, we discovered that hyaluronan can effectively compete with hIgG to bind with *ct*GNP. Several lines of experimental evidence are presented here. In a first experiment, HA with a low molecular weight of 29 kDa (HAL) was mixed with hIgG or hIgM

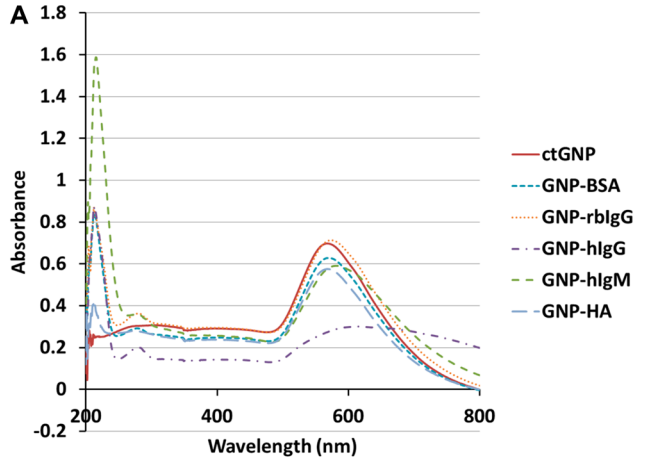

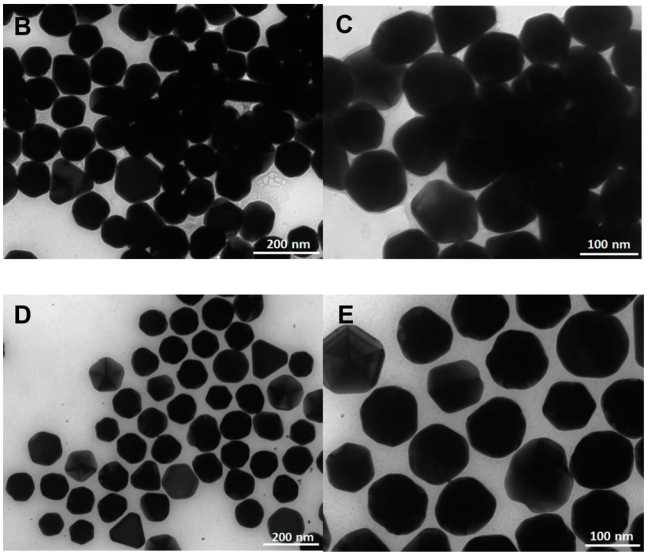

Figure 3. (A) UV−vis absorption spectra of *ct*GNP upon adsorption of various biomolecules. The mixture solution was prepared by adding 20 μL of biomolecule solution at a fixed weight concentration of 1 mg/mL to 400 μL of *ct*GNP solution. (B−E): Representative TEM images of hIgG (B and C) and hIgM (D and E) interaction products with *ct*GNP.

solution at different concentrations. The concentration of hIgG and hIgM was 1 mg/mL. The final concentration of HAL in the mixed solutions was 0, 0.005, 0.05, and 0.5 mg/mL, respectively. The presence of HAL in hIgG solution led to a substantially reduced average nanoparticle size compared to the pure hIgG solution (Figure 4A). Even at 0.005 mg/mL (0.5% of the hIgG concentration), HAL still caused a visible nanoparticle size reduction. In contrast, no significant difference was observed from the pure hIgM and mixed HAL/hIgM solutions, even at a weight concentration as high as 0.5 mg/mL (Figure 4B).

The size reduction caused by HA in the hIgG adsorption assay could be due to two reasons: (1) competition between HA with hIgG to bind with the *ct*GNPs, or (2) interaction between HA and hIgG, preventing hIgG from binding with *ct*GNPs. To identify which possibility is the case, we first mixed 25 μL of HAL at a concentration of 1 mg/mL with 500 μL of *ct*GNP, and then purified the conjugation product by centrifuge and washing with water. The average diameter of the HA-modified GNP increased by about 10 nm compared to the

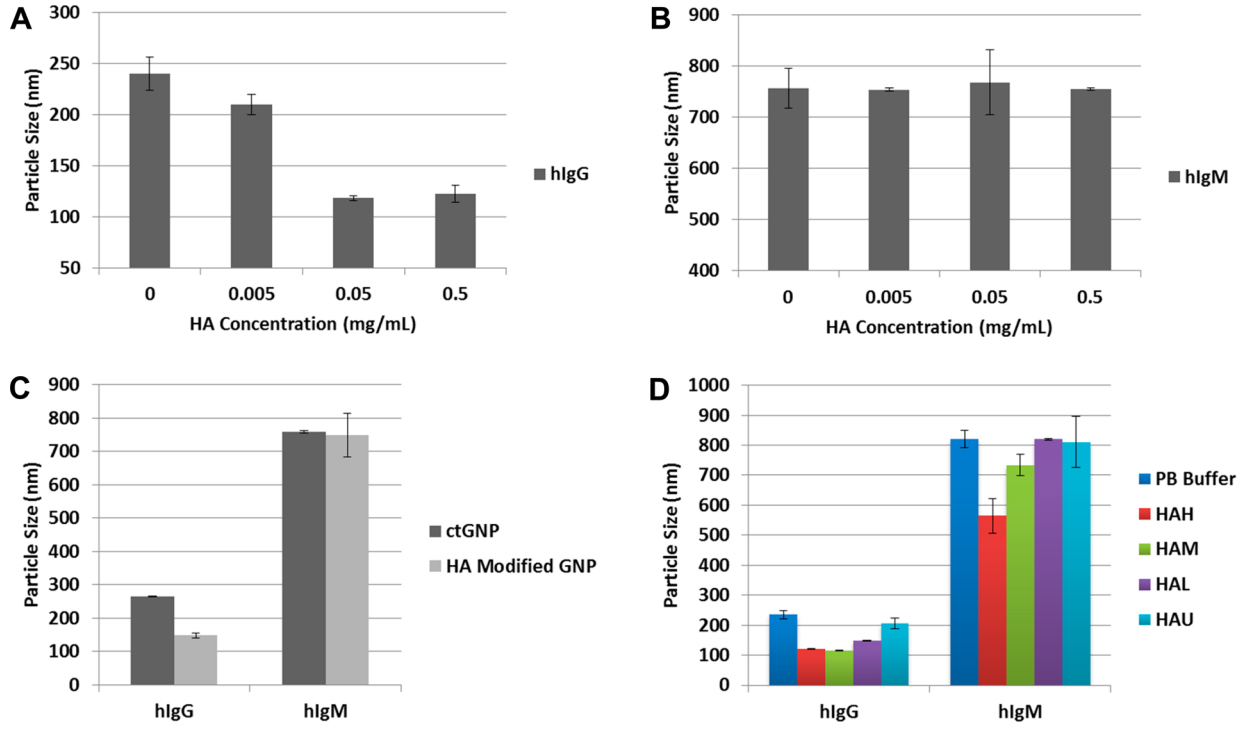

Figure 4. Effect of hyaluronan (HA) on hIgG and hIgM interaction with *ct*GNP. (A) GNP adsorption assay of hIgG treated with low molecular weight HAL (M.W. 29 kDa) at different concentrations. One microliter of HAL solution at a concentration of 0, 0.1, 1, or 10 mg/mL was mixed with 20 μL of hIgG solution (1 mg/mL). A same amount of phosphate buffer (PB) was added into hIgG as a negative control. The final concentration of HAL in hIgG solution is 0, 0.005, 0.05, or 0.5 mg/mL, respectively. The mixture solution was incubated at room temperature for 30 min before average particle size was measured. (B) Same study conducted on hIgM. (C) Interaction of hIgG and hIgM with HA-modified GNPs. Twenty-five microliters of HAL solution at 1 mg/mL was first mixed with 500 μL of *ct*GNP solution. After incubation for 30 min, the conjugate solution was centrifuged at 5000 rpm for 3 min and the clear supernatant was discarded. The GNP residue was washed with pure water once, centrifuged, and then redispersed in 500 μL of nanopure deionized water. Two microliters of hIgG or hIgM at 1 mg/mL was added into 40 μL of the HA-modified GNP solution. Average particle size was measured following a 6 min of incubation time. (D) Effect of molecular weight of HA on hIgG and hIgM interaction with *ct*GNP. To conduct the assay, 1 μL of HA solution of different molecular weights at a weight concentration of 1 mg/mL was mixed with 20 μL of hIgG or hIgM solution (1 mg/mL). Same amount of PB buffer was added into hIgG or hIgM as a negative control. Following a 30 min of incubation time, particle size analysis was conducted.

*ct*GNP, same as observed without centrifuge. After being redispersed in solution, hIgG or hIgM was added to the HA-modified GNP. With the addition of hIgG, the particle size increased only by ~20−30 nm, a substantially smaller size increase compared to the pure hIgG-*ct*GNP adsorption assay, which is typically ~250 nm. With the addition of hIgM, the particle size increased to about 700 nm, which is comparable to the adsorption of pure hIgM with *ct*GNP (Figure 4C). The centrifuge of HA-modified GNP eliminated the potential interaction of HA with hIgG or hIgM in solution. This leaves competitive adsorption of HA with hIgG as the only possible mechanism for the reduced average particle size in the nanoparticle adsorption assay.

In a third experiment, we compared the molecular weight effect of HA on hIgG and hIgM−*ct*GNP adsorption. One microliter of HA of different molecular weights at the same weight concentration of 1 mg/mL was added to 20 μL of hIgG or hIgM solution (1 mg/mL). The molar concentration of HA increases from HAH to HAU accordingly. Size measurement reveals that higher molecular weight HA exhibited more profound effect on the adsorption of hIgG to *ct*GNP. There is almost no effect observed from the ultralow molecular weight HAU, despite the fact that this HA has the highest molar concentration in the mixture solution (Figure 4D). As for the hIgM−*ct*GNP adsorption, low and ultralow molecular weight HAL and HAU had no effect on the average particle size, but high and medium molecular weight HAH and HAM resulted in a visible size reduction.

These competitive adsorption studies revealed several important mechanistic aspects not only on how HA but also on how hIgG and hIgM interact with *ct*GNP. When hIgG was added to the HA-modified *ct*GNP, hIgG could no longer cross-link *ct*GNP into aggregates. This fact suggests that hIgG must interact directly with the metal core during its interaction with *ct*GNP. The interaction between hIgG and *ct*GNP is not based on electrostatic interaction between the positive charge from hIgG and the citrate ligands. HA-modified GNP has a similar ζ-potential as *ct*GNP (Figure 3C). If hIgG interacts with the citrate ligands by electrostatic interaction, it would interact with the HA-modified GNPs as well.

The effect of HA on hIgM-*ct*GNP adsorption assay is rather interesting. From the second experiment, the adsorption study of hIgG with HA-modified GNP, it is confirmed that HA is adsorbed to the *ct*GNP. However, the formation of a new HA layer on the GNP does not change the interaction of hIgM with the GNP. Only one possible mechanism can explain this result: hIgM interacts with the *ct*GNP or HA-modified GNP by forming electrostatic interaction with the negative charged citrate ligands or HA on the gold nanoparticle surface. hIgM does not displace the citrate ligands during the interaction. Because the gold nanoparticle maintains its citrate protection layer during the interaction with hIgM, the nanoparticles

remain stable, and no coalescence occurs as a result of interaction with hIgM. This interaction mode is also supported by the previously discussed UV−vis absorption and TEM study.

The different molecular weight effects of HA on hIgG-*ct*GNP adsorption suggest that the strong binding affinity of HA with the *ct*GNP is associated with its linear polymer chain length: the longer polymer chain of HA can form more "interaction points" with the nanoparticle, and as a result, forms a stronger binding with the *ct*GNP. The ultralow molecular weight HAU cannot form sufficient contact points with the *ct*GNP, therefore, lacks the ability to bind with *ct*GNPs tightly. According to recent studies by Iosin et al.[28] and Maleki et al.,[29] protein binding to *ct*GNP is a spontaneous process with a negative Gibbs free energy change, ΔG. The enthalpy change ΔH of the reaction is negative, and the entropy of the system ΔS is decreased. During the interaction, the adsorption of protein to the nanoparticle leads to an entropy decrease, while the release of citrate ions to solution leads to an entropy increase. The net result is a slight decrease of the entropy. Enthalpy change ΔH is the main contributor to the negative ΔG. A longer HA polymer chain should be able to form more interaction points with the *ct*GNPs, leading to a more negative enthalpy change of the interaction, thus favoring the binding product formation. With medium and high molecular weight HAH and HAM, we also see a particle size reduction effect on the hIgM−*ct*GNP adsorption assay; however, the relative effect of this size reduction is much lesser than the hIgG−*ct*GNP adsorption. Even with HAH, the average particle size of the hIgM−*ct*GNP adsorption product remains around 500−600 nm, indicating the presence of a substantial amount of nanoparticle clusters. Although HA is highly negatively charged like citrate, there are some major structural differences between HA and citrate ligands. After the coating of *ct*GNP by HA layer, it is possible that the binding affinity of hIgM with HA-modified GNPs is slightly lower than *ct*GNP, leading to a slight particle size reduction.

Stability Study of *ct*GNP Treated with BSA, HA, and rbIgG at Increased Salt Conditions. *ct*GNPs are not stable in high salt conditions because the electrolytes can lead to the disruption of electrostatic interactions between the citrate ligands and the nanoparticle core, causing irreversible nanoparticle aggregation to occur. However, if the nanoparticle surface is covered by a closely packed protein corona, the modified gold nanoparticle becomes stabilized in high salt solutions. This phenomenon has often been used as a practical method to confirm if a protein is successfully conjugated with the *ct*GNPs by adsorption.[16] To use the gold nanoparticle bioconjugate in biological fluids and specimens, it is required that the nanoparticle conjugate remains to be stable at physiological condition which usually has a salt concentration of 100−200 mM. Here we examined the salt effect on BSA, HA, and rbIgG-treated GNPs. Because hIgG and hIgM are causing continuous particle size increase when mixed with *ct*GNPs, this study was not conducted on hIgG or hIgM-treated GNP.

Among BSA, rbIgG, and HA, only BSA-treated GNP showed almost no particle size change upon addition of NaCl, whereas the other two exhibit significant size increases over time (Figure 5A). This result could be interpreted as that the *ct*GNP is fully covered by a tightly enclosed BSA monolayer, whereas the coverage of the *ct*GNP by IgG or HA is only partial. The tightly enclosed BSA monolayer formation should be associated with a strong interaction between the BSA molecules. Although rbIgG and HA also formed an adsorbed layer on the nanoparticle surface, the biomolecular layer is not fully enclosed and the interaction is largely based on electrostatic interactions between the biomolecule and the nanoparticle surface. The diffusion of Na^+ ions through the biomolecular layer destroys the IgG or HA−*ct*GNP interaction, leading to irreversible nanoparticle aggregate formation. Another result to be noted here is that the stability of IgG or HA coated GNP appears to be even worse than the *ct*GNP. This indicates that HA or rbIgG interacts with *ct*GNP and breaks the citrate layer, likely by displacing the citrate and direct interacting with the metal core.

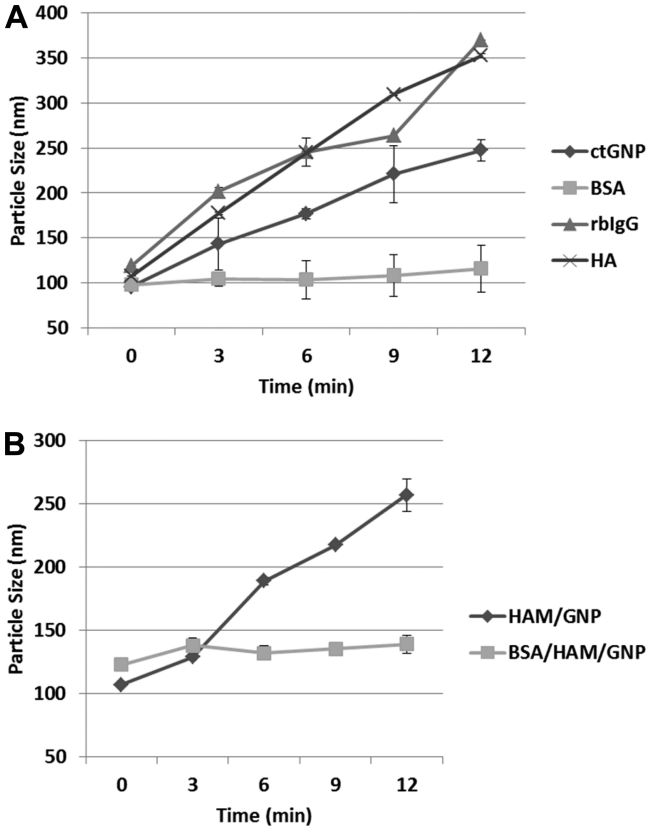

Figure 5. Stability study of *ct*GNP, biomolecule-coated GNP and HA modified GNP at increased salt concentrations. (A) Salt effect on BSA, rbIgG, and HA-coated GNP. BSA, rbIgG, and HA coated GNP was prepared by adding 2 μL of corresponding biomolecule solution at a concentration of 1 mg/mL to 40 μL of ctGNP solution. The average particle size of these mixed solutions remained stable for days. To examine the salt effect, 2 μL of a 5× concentrated PBS solution was added to the above mixed biomolecule−GNP solutions, followed by particle size detection over a 12 min period. The final concentration of NaCl in the mixed biomolecule−GNP solutions is 40 mM. (B) Stability study of HA-modified GNP followed by additional BSA adsorption. HA modified GNP was prepared according to the same protocol as described in Figure 4C. Two microliters of BSA at a concentration of 1 mg/mL was then added to 40 μL of HA-modified GNP solution. The particle size was determined following a 3 min of incubation. Then, 2 μL of a 5× concentrated PBS solution was added, followed by particle size measurement over a 12 min period. The final concentration of NaCl in the mixture solution is 40 mM.

An additional salt-stability study performed on HA-modified GNP followed by adsorption of BSA revealed further insights on the binding mode between BSA and *ct*GNP. In this experiment, *ct*GNP was first modified with a layer of HAM as discussed earlier in Figure 4C. When BSA was added to this

HAM-modified GNP, the average particle size was increased by about 10 nm. This size increase corresponds approximately to twice of the diameter of BSA. Following the addition of NaCl solution, the nanoparticle exhibited a high stability very similar to BSA directly coated GNPs (Figure 5B). This result suggests that BSA is adsorbed to the HA-modified GNP, leading to the formation of a "double layer" corona on the GNP surface. It is to be recalled that the ζ-potential of HA-treated GNP is −40 mV, confirming that the nanoparticle is highly negatively charged (Figure 2C). The fact that BSA can readily adsorb to either citrate or HA-coated GNP suggests that the interaction between BSA and *ct*GNP or HA−GNP is primarily electrostatic interaction between BSA and the negatively charged ligands on the nanoparticle surface. Study reported by Brewer et al. using quartz crystal microbalance and ζ-potential measurements also concludes that BSA interacts with the citrate ligands on *ct*GNP through electrostatic interactions.[25] Furthermore, the fact that such interactions between BSA and the nanoparticles are not destroyed by the addition of high concentration salt suggests that the exceptional stability of BSA-modified GNP must arise from the strong interactions between BSA molecules within the protein layer, not between the BSA and the nanoparticle.

The measured ζ-potential of BSA in pure water is about −20 mV; therefore, BSA is overall negatively charged. The interaction between negatively charged BSA and negatively charged GNP appears to be counterintuitive in the first sight. However, extensive literature reports have confirmed that BSA can interact with polyanions such as poly(acrylic acid) or negatively charged proteins through the positively charged "patches" on BSA.[25,48,49] The uneven distribution of surface charge on proteins adds extra complexity to the interaction between a protein and nanoparticle materials. It is completely possible that a protein, regardless what its isoelectric point is, and the pH condition of the solution, could interact with both positively or negatively charged nanoparticles.

CONCLUSIONS

From this study, we identified at least five possible interaction modes from different biomolecules and citrate-capped gold nanoparticles. Four proteins and one negatively charged polysaccharide were investigated in this study. There are two findings made from this study that are particularly noteworthy. First, contrary to a popular belief that during the protein−*ct*GNP interaction, the citrate ligands are displaced by the protein, this assumption is not always true. Our study finds that both BSA and IgM interact directly with the negatively charged ligands on the gold nanoparticles. On the other hand, IgG type protein appears to displace the citrate ligands to bind with the metal core during its interaction with the *ct*GNP. Second, HA, a highly negatively charged polysaccharide, has an exceptionally high affinity with the *ct*GNP and it can effectively compete with other serum proteins to bind with *ct*GNPs. An elevated HA level is closely associated with tumor progression and metastasis. Our finding leads to an exciting implication that the composition of the biomolecular corona formed on the *ct*GNPs placed in blood serum or other biological fluids could reflect some pathological conditions of an individual, and the analysis of these compositions could potentially lead to new biomarker discovery. It has been suggested or demonstrated that the composition of the biomolecular corona may be used to "fingerprint" biological processes and molecular mechanisms with diagnostic and therapeutic significance.[22,23,50,51]

In summary, due to the complex and flexible structures of biomolecules, especially proteins, the interaction between biomolecules and nanoparticle materials could be very complicated. Further studies are needed to understand various biomolecular-nanoparticle interactions at a more extensive level. These studies will not only provide guidance to prepare better nanoparticle bioconjugates and lead to better understanding on the in vivo behavior of nanoparticle materials but also will potentially bring new advancements in molecular diagnostics.

MATERIALS AND METHODS

Chemical and Biochemical Reagents. Citrate-protected gold nanoparticle (GNP) (15708-9) was purchased from Ted Pella Inc. (Redding, CA). The average diameter of the citrate GNP is about 95 nm and the concentration of the nanoparticle is 10 pM. Human IgG (ab91102), human IgM (ab91117), and rabbit polyclonal antihuman IgG (ab6715) were purchased from Abcam (Cambridge, MA). Hyaluronan of four different molecular weights (GLR003, M.W. 7 kDa; GLR001, M.W. 29 kDa; GLR004, M.W. 289 kDa; GLR002, M.W. 1.5 MDa) were purchased from R&D Systems (Minneapolis, MN). Bovine serum albumin (A7030) and all other chemicals were purchased from Sigma (Saint Louis, MO).

Sample Preparation and Assay Procedures. In general, to conduct the nanoparticle adsorption assay, 2 μL of prepared sample solution was mixed with 40 μL of GNP solution. The average particle size of the assay solution was measured after 6 min of incubation, or as specified in the figure captions. All assays were conducted at least in duplicate and the error bars in each plot represent the standard deviation of the assay results. Specific sample preparation protocols can be found in the corresponding figure captions.

Dynamic Light Scattering (DLS) Analysis. All particle size analysis in this study was conducted using an automatic NDS1200 DLS instrument from Nano Discovery Inc. (Orlando, FL). This system is equipped with a 633 nm He−Ne laser (0.5 mW) and a 12-sample holder, which allows the measurement of 12 samples within 6 min. All DLS measurements were conducted at an ambient temperature of 25 °C.

ζ-Potential Analysis. ζ-Potential analysis was conducted using a Zetasizer Nano ZS90 instrument from Malvern Instruments Ltd. (Westborough, MA). It is equipped with laser doppler micro-electrophoresis that can be used to measure ζ-potential. To measure the ζ-potential of biomolecule-treated GNPs, 2 μL of sample solution was mixed with 600 μL of *ct*GNPs, followed by 3 measurements. Each measurement result was calculated from the average of 12 runs and each run takes up to 30 s to complete. The error bars in each plot represent the standard deviation of each 3 measurements.

UV−Vis Absorption Spectra. UV−vis absorption analysis was conducted using a Cary Win UV spectrometer from Agilent Technologies (Santa Clara, CA). This spectrometer measures the transmission/absorbance spectra using double beam principle. To analyze the UV−vis absorption spectra of biomolecule-treated GNP, 20 μL of biomolecule solution was mixed with 400 μL of GNPs. Following 6 min of incubation, spectra were measured.

Transmission Electron Microscope (TEM) Analysis. The TEM analysis was conducted using a TEM-1011 microscope from JEOL Ltd., which is equipped with 0.2 nm line resolution and 0.4 nm point resolution. The *ct*GNPs used for TEM analysis was first concentrated 10 times before mixing with protein solutions. 400 square mesh gold grids (FF400-Au) from Electron Microscopy Sciences (Hatfield, PA) were used for the experiments. To prepare sample on the grids, 2 μL of prepared protein−*ct*GNP solution was placed on the grid and allowed to dry completely at room temperature before being analyzed by TEM.

■ ASSOCIATED CONTENT

Supporting Information

Size exclusion chromatography analysis of human IgG (Figure S1). Lower magnification TEM images of *ct*GNP, hIgG−*ct*GNP, and hIgM−*ct*GNP interaction products (Figure S2). This material is available free of charge via the Internet at http://pubs.acs.org/.

■ AUTHOR INFORMATION

Corresponding Author

*Q. Huo. E-mail: Qun.Huo@ucf.edu. Tel: 407-882-2845.

Notes

The authors declare no competing financial interest.

■ REFERENCES

(1) Turkevich, J.; Stevenson, P. C.; Hillier, J. A Study of the Nucleation and Growth Processes in the Synthesis of Colloidal Gold. *Discuss. Faraday Soc.* **1951**, *11*, 55−75.

(2) Kimling, J.; Maier, M.; Okenve, B.; Kotaidis, V.; Ballot, H.; Plech, A. Turkevich Method for Gold Nanoparticle Synthesis Revisited. *J. Phys. Chem. B* **2006**, *110*, 15700−15707.

(3) Frens, G. Particle Size and Sol Stability in Metal Colloids. *Kolloid Z. Z. Polym.* **1972**, *250*, 736−741.

(4) Frens, G. Controlled Nucleation for the Regulation of the Particle Size in Monodisperse Gold Suspensions. *Nature* **1973**, *241*, 20−22.

(5) Boisselier, E.; Astruc, D. Gold Nanoparticles in Nanomedicine: Preparations, Imaging, Diagnostics, Therapies and Toxicity. *Chem. Soc. Rev.* **2009**, *38*, 1759−1782.

(6) Jans, H.; Huo, Q. Gold Nanoparticle-Enabled Biological and Chemical Detection and Analysis. *Chem. Soc. Rev.* **2012**, *41*, 2849−2866.

(7) Rahman, M.; Laurent, S.; Tawil, N.; Yahia, L. H.; Mahmoudi, M. Nanoparticle and Protein Corona. In *Protein-Nanoparticle Interactions*; Springer: New York, 2013; pp 21−44.

(8) Walkey, C. D.; Chan, W. C. Understanding and Controlling the Interaction of Nanomaterials with Proteins in a Physiological Environment. *Chem. Soc. Rev.* **2012**, *41*, 2780−2799.

(9) Cui, M.; Liu, R.; Deng, Z.; Ge, G.; Liu, Y.; Xie, L. Quantitative Study of Protein Coronas on Gold Nanoparticles with Different Surface Modifications. *Nano Res.* **2014**, *7*, 345−352.

(10) Dobrovolskaia, M. A.; Patri, A. K.; Zheng, J.; Clogston, J. D.; Ayub, N.; Aggarwal, P.; Neun, B. W.; Hall, J. B.; McNeil, S. E. Interaction of Colloidal Gold Nanoparticles with Human Blood: Effects on Particle Size and Analysis of Plasma Protein Binding Profiles. *Nanomedicine* **2009**, *5*, 106−117.

(11) Lacerda, S. H. D. P.; Park, J. J.; Meuse, C.; Pristinski, D.; Becker, M. L.; Karim, A.; Douglas, J. F. Interaction of Gold Nanoparticles with Common Human Blood Proteins. *ACS Nano* **2009**, *4*, 365−379.

(12) Chithrani, B. D.; Ghazani, A. A.; Chan, W. C. Determining the Size and Shape Dependence of Gold Nanoparticle Uptake into Mammalian Cells. *Nano Lett.* **2006**, *6*, 662−668.

(13) Calzolai, L.; Franchini, F.; Gilliland, D.; Rossi, F. Protein−Nanoparticle Interaction: Identification of the Ubiquitin−Gold Nanoparticle Interaction Site. *Nano Lett.* **2010**, *10*, 3101−3105.

(14) Bendayan, M. Worth Its Weight in Gold. *Science* **2001**, *291*, 1363−1365.

(15) De Mey, J. Colloid Gold Probes in Immunocytochemistry. In *Immunocytochemistry − Practical Applications in Pathology and Biology*; Polak, J. M., Van Norden, S., Eds.; Wright: Bristol, U. K., 1983.

(16) Hermanson, G. T. *Bioconjugate Techniques*, 2nd ed.; Pierce Biotechnology, Thermo Fisher Scientific: Rockford, IL, 2008; Chapter 24.

(17) Krebs, H. Chemical Composition of Blood Plasma and Serum. *Annu. Rev. Biochem.* **1950**, *19*, 409−430.

(18) Anderson, N. L.; Polanski, M.; Pieper, R.; Gatlin, T.; Tirumalai, R. S.; Conrads, T. P.; Veenstra, T. D.; Adkins, J. N.; Pounds, J. G.; Fagan, R. The Human Plasma Proteome a Nonredundant List Developed by Combination of Four Separate Sources. *Mol. Cell. Proteomics* **2004**, *3*, 311−326.

(19) Nedelkov, D.; Phillips, D. A.; Tubbs, K. A.; Nelson, R. W. Investigation of Human Protein Variants and Their Frequency in the General Population. *Mol. Cell. Proteomics* **2007**, *6*, 1183−1187.

(20) Stoica, G.; Macarie, E.; Michiu, V.; Stoica, R. Biologic Variation of Human Immunoglobulin Concentration. I. Sex-Age Specific Effects on Serum Levels of IgG, IgA, IgM and IgD. *Med. Interne* **1979**, *18*, 323−332.

(21) Whitney, A. R.; Diehn, M.; Popper, S. J.; Alizadeh, A. A.; Boldrick, J. C.; Relman, D. A.; Brown, P. O. Individuality and Variation in Gene Expression Patterns in Human Blood. *Proc. Natl. Acad. Sci. U. S. A.* **2003**, *100*, 1896−1901.

(22) Huo, Q.; Colon, J.; Cordero, A.; Bogdanovic, J.; Baker, C. H.; Goodison, S.; Pensky, M. Y. A Facile Nanoparticle Immunoassay for Cancer Biomarker Discovery. *J. Nanobiotechnol.* **2011**, *9*, 20.

(23) Huo, Q.; Litherland, S. A.; Sullivan, S.; Hallquist, H.; Decker, D. A.; Rivera-Ramirez, I. Developing a Nanoparticle Test for Prostate Cancer Scoring. *J. Transl. Med.* **2012**, *10*, 44.

(24) Tsai, D.-H.; DelRio, F. W.; Keene, A. M.; Tyner, K. M.; MacCuspie, R. I.; Cho, T. J.; Zachariah, M. R.; Hackley, V. A. Adsorption and Conformation of Serum Albumin Protein on Gold Nanoparticles Investigated Using Dimensional Measurements and in Situ Spectroscopic Methods. *Langmuir* **2011**, *27*, 2464−2477.

(25) Brewer, S. H.; Glomm, W. R.; Johnson, M. C.; Knag, M. K.; Franzen, S. Probing BSA Binding to Citrate-Coated Gold Nanoparticles and Surfaces. *Langmuir* **2005**, *21*, 9303−9307.

(26) Glomm, W. R.; Halskau, Ø.; Hanneseth, A.-M. D.; Volden, S. Adsorption Behavior of Acidic and Basic Proteins onto Citrate-Coated Au Surfaces Correlated to Their Native Fold, Stability, and PI. *J. Phys. Chem. B* **2007**, *111*, 14329−14345.

(27) Shang, L.; Wang, Y.; Jiang, J.; Dong, S. pH-Dependent Protein Conformational Changes in Albumin: Gold Nanoparticle Bioconjugates: A Spectroscopic Study. *Langmuir* **2007**, *23*, 2714−2721.

(28) Iosin, M.; Canpean, V.; Astilean, S. Spectroscopic Studies on pH- and Thermally Induced Conformational Changes of Bovine Serum Albumin Adsorbed onto Gold Nanoparticles. *J. Photochem. Photobiol., A* **2011**, *217*, 395−401.

(29) Maleki, M. S.; Moradi, Q.; Tahmasebi, S. Adsorption of Albumin by Gold Nanoparticles: Equilibrium and Thermodynamics Studies. *Arabian J. Chem.* **2013**; published online (open access).

(30) Tankersley, D. L.; Preston, M. S.; Finlayson, J. Immunoglobulin G Dimer: An Idiotype-Anti-Idiotype Complex. *Mol. Immunol.* **1988**, *25*, 41−48.

(31) Roux, K. H.; Tankersley, D. L. A View of the Human Idiotypic Repertoire. Electron Microscopic and Immunologic Analyses of Spontaneous Idiotype-Anti-Idiotype Dimers in Pooled Human IgG. *J. Immunol.* **1990**, *144*, 1387−1395.

(32) Gronski, P. IgG Dimers in Multidonor-Derived Immunoglobulins: Aspects of Generation and Function. *Curr. Pharm. Des.* **2006**, *12*, 181−190.

(33) Stern, R. *Hyaluronan in Cancer Biology*. Academic Press: 2009.

(34) Bharadwaj, A. G.; Kovar, J. L.; Loughman, E.; Elowsky, C.; Oakley, G. G.; Simpson, M. A. Spontaneous Metastasis of Prostate Cancer Is Promoted by Excess Hyaluronan Synthesis and Processing. *Am. J. Pathol.* **2009**, *174*, 1027−1036.

(35) Lipponen, P.; Aaltomaa, S.; Tammi, R.; Tammi, M.; Ågren, U.; Kosma, V.-M. High Stromal Hyaluronan Level is Associated with Poor Differentiation and Metastasis in Prostate Cancer. *Eur. J. Cancer* **2001**, *37*, 849−856.

(36) Lokeshwar, V. B.; Öbek, C.; Pham, H. T.; Wei, D.; Young, M. J.; Duncan, R. C.; Soloway, M. S.; Block, N. L. Urinary Hyaluronic Acid and Hyaluronidase: Markers for Bladder Cancer Detection and Evaluation of Grade. *J. Urol. (N. Y., NY, U. S.)* **2000**, *163*, 348−356.

(37) Lokeshwar, V. B.; Öbek, C.; Soloway, M. S.; Block, N. L. Tumor-Associated Hyaluronic Acid: A New Sensitive and Specific Urine Marker for Bladder Cancer. *Cancer Res.* **1997**, *57*, 773−777.

(38) Kemp, M. M.; Kumar, A.; Mousa, S.; Park, T.-J.; Ajayan, P.; Kubotera, N.; Mousa, S. A.; Linhardt, R. J. Synthesis of Gold and Silver

Nanoparticles Stabilized with Glycosaminoglycans Having Distinctive Biological Activities. *Biomacromolecules* **2009**, *10*, 589−595.
(39) Lee, H.; Lee, K.; Kim, I. K.; Park, T. G. Synthesis, Characterization, and in Vivo Diagnostic Applications of Hyaluronic Acid Immobilized Gold Nanoprobes. *Biomaterials* **2008**, *29*, 4709−4718.
(40) Lee, M.-Y.; Yang, J.-A.; Jung, H. S.; Beack, S.; Choi, J. E.; Hur, W.; Koo, H.; Kim, K.; Yoon, S. K.; Hahn, S. K. Hyaluronic Acid−Gold Nanoparticle/Interferon A Complex for Targeted Treatment of Hepatitis C Virus Infection. *ACS Nano* **2012**, *6*, 9522−9531.
(41) James, A. E.; Driskell, J. D. Monitoring Gold Nanoparticle Conjugation and Analysis of Biomolecular Binding with Nanoparticle Tracking Analysis (NTA) and Dynamic Light Scattering (DLS). *Analyst* **2013**, *138*, 1212−1218.
(42) Jans, H.; Liu, X.; Austin, L.; Maes, G.; Huo, Q. Dynamic Light Scattering as a Powerful Tool for Gold Nanoparticle Bioconjugation and Biomolecular Binding Studies. *Anal. Chem.* **2009**, *81*, 9425−9432.
(43) Austin, L.; Liu, X.; Huo, Q. An Immunoassay for Monoclonal Antibody Isotyping and Quality Analysis Using Gold nanoparticles and Dynamic Light Scattering. *Am. Biotechnol. Lab.* **2010**, *28*, 10−12.
(44) Bohidar, H. Light Scattering Study of Solution Properties of Bovine Serum Albumin, Insulin, and Polystyrene under Moderate Pressure. *Colloid Polym. Sci.* **1989**, *267*, 292−300.
(45) Jøssang, T.; Feder, J.; Rosenqvist, E. Photon Correlation Spectroscopy of Human IgG. *J. Protein Chem.* **1988**, *7*, 165−171.
(46) Bogdanovic, J.; Colon, J.; Baker, C.; Huo, Q. A Label-Free Nanoparticle Aggregation Assay for Protein Complex/Aggregate Detection and Study. *Anal. Biochem.* **2010**, *405*, 96−102.
(47) Cowman, M. K.; Matsuoka, S. Experimental Approaches to Hyaluronan Structure. *Carbohydr. Res.* **2005**, *340*, 791−809.
(48) Park, J. M.; Muhoberac, B. B.; Dubin, P. L.; Xia, J. Effects of Protein Charge Heterogeneity in Protein-Polyelectrolyte Complexation. *Macromolecules* **1992**, *25*, 290−295.
(49) Tribet, C.; Porcar, I.; Bonnefont, P.; Audebert, R. Association between Hydrophobically Modified Polyanions and Negatively Charged Bovine Serum Albumin. *J. Phys. Chem. B* **1998**, *102*, 1327−1333.
(50) Walkey, C. D.; Olsen, J. B.; Song, F.; Liu, R.; Guo, H.; Olsen, D. W. H.; Cohen, Y.; Emili, A.; Chan, W. C. W. Protein Corona Fingerprinting Predicts the Cellular Interaction of Gold and Silver Nanoparticles. *ACS Nano* **2014**, *8*, 2439−2455.
(51) Monopoli, M. P.; Aberg, C.; Salvati, A.; Dawson, K. A. Biomolecular Coronas Provide the Biological Identity of Nanosized Materials. *Nat. Nanotechnol.* **2012**, *7*, 779−786.